Heterogeneous Catalysis

Zeolite-Tailored Active Site Proximity for the Efficient Production of Pentanoic Biofuels

Jiang He[+], Zhijie Wu[+], Qingqing Gu[+], Yuanshuai Liu, Shengqi Chu, Shaohua Chen, Yafeng Zhang, Bing Yang, Tiehong Chen, Aiqin Wang, Bert M. Weckhuysen,* Tao Zhang,* and Wenhao Luo*

Abstract: Biofuel production can alleviate reliance on fossil resources and thus carbon dioxide emission. Hydrodeoxygenation (HDO) refers collectively to a series of important biorefinery processes to produce biofuels. Here, well-dispersed and ultra-small Ru metal nanoclusters (ca. 1 nm), confined within the micropores of zeolite Y, provide the required active site intimacy, which significantly boosts the chemoselectivity towards the production of pentanoic biofuels in the direct, one-pot HDO of neat ethyl levulinate. Crucial for improving catalyst stability is the addition of La, which upholds the confined proximity by preventing zeolite lattice deconstruction during catalysis. We have established and extended an understanding of the "intimacy criterion" in catalytic biomass valorization. These findings bring new understanding of HDO reactions over confined proximity sites, leading to potential application for pentanoic biofuels in biomass conversion.

Introduction

The finite reserve of non-renewable fossil resources, such as coal, natural gas, and crude oil, and the growing global energy demand, combined with increasingly stringent legislation and mandates on CO_2 emissions, have prompted the wide-ranging search for alternative feedstocks and necessity of driving the essential transition to a more renewables-based, sustainable society.[1] Non-edible biomass is one prime, renewable and abundant carbon-based alternative, which can serve as a viable substitute for the sustainable production of fuels, chemicals and materials. The exploration and

development of biomass for sustainable energy production, including the manufacturing of biofuels and bio-based additives, such as lubricants, can be a promising option for the energy sector.[2] Additionally, there is a clear tendency towards increasing utilization of renewables for the transportation sector for alleviating our reliance on fossil resources, further spurred by the rising concerns about climate change.[3]

The current implemented option is using bio-ethanol as a blend with gasoline, which is widely applied in China and several European countries (i.e., E10, referring to a 10% blend of ethanol).[4] However, limitations referring to a lower energy density and inferior compatibility, compared to that of traditional gasoline, lead to an ongoing debate about developing alternatives for bio-ethanol. To this end, alternative molecules, such as pentanoic esters, produced from lignocellulose-derived levulinic acid (LA) have been identified as a promising class of biofuels (additives) by Shell laboratories.[5] An example is ethyl pentanoate (EP) at a 15 vol% blend with fossil-derived gasoline, representing superior fuel properties and excellent compatibility with existing combustion engines, as evidenced by a successful road trial of 250 000 km. The reported production of EP from lignocellulose-derived downstream platform molecule of LA, consists of the hydrogenation of LA to γ-valerolactone (GVL) and subsequently into pentanoic acid (PA), and finally esterification to EP (Scheme 1). Metal/zeolite bifunctional catalysts with considerable activity and selectivity for LA hydrodeoxygenation (HDO) has been developed for the efficient production of pentanoic biofuels.[6] However, the developed

---

[*] J. He,[+] Dr. B. Yang, Prof. A. Wang, Prof. T. Zhang, Dr. W. Luo
CAS Key Laboratory of Science and Technology on Applied Catalysis,
Dalian Institute of Chemical Physics, Chinese Academy of Sciences
457 Zhongshan Road, Dalian, 116023 (P. R. China)
E-mail: taozhang@dicp.ac.cn
w.luo@dicp.ac.cn

J. He[+]
University of Chinese Academy of Science
19A Yuquan Road, Shijingshan District, Beijing, 100049 (P. R. China)

Prof. Z. Wu[+]
State Key Laboratory of Heavy Oil Processing and Key Laboratory of
Catalysis of CNPC, China University of Petroleum
18 Fuxue Road, ChangPing, Beijing, 102249 (P. R. China)

Dr. Q. Gu,[+] Dr. Y. Zhang, Dr. B. Yang
Dalian National Laboratory for Clean Energy, Dalian Institute of
Chemical Physics, Chinese Academy of Sciences
457 Zhongshan Road, Dalian, 116023 (P. R. China)

Dr. Y. Liu, Prof. B. M. Weckhuysen
Inorganic Chemistry and Catalysis group
Debye Institute for Nanomaterials Science, Utrecht University
Universiteitsweg 99, 3584 CG Utrecht (The Netherlands)
E-mail: B.M.Weckhuysen@uu.nl

Dr. S. Chu
Beijing Synchrotron Radiation Facility
Institute of High Energy Physics, Chinese Academy of Sciences
19B Yuquan Road, Shijingshan District, Beijing, 100049 (P. R. China)

Dr. S. Chen, Prof. T. Chen
Key Laboratory of Advanced Energy Materials Chemistry
Institute of New Catalytic Materials Science, Nankai University
38 Tongyang Road, Tianjin, 300350 (P. R. China)

[+] These authors contributed equally to this work.

Supporting information and the ORCID identification number(s) for
the author(s) of this article can be found under:
https://doi.org/10.1002/anie.202108170.
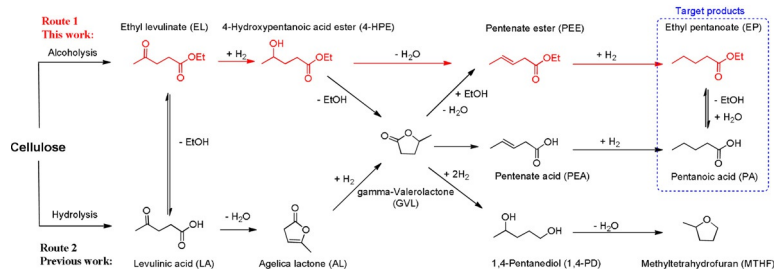
Scheme 1. The production of pentanoic biofuels starting from ethyl levulinate (route 1: the proposed synthesis route described in this work) and levulinic acid (route 2: the previously reported synthesis process).

catalysts still encompass several challenges, with respect to 1) the lack of precision synthesis methods enabling the active site control at the nanometric level; 2) unpractical dilute substrate solutions; and 3) underestimated aspects on catalyst stability as the highly oxygen-functionalized, polar, and even corrosive reaction medium under applied elevated temperatures often results in a poor durability of the solid catalysts studied. Therefore, there is clear room in developing more stable and well-defined bifunctional catalysts via rational design approaches, operating under more demanding experimental conditions.

In this work, we propose a novel strategy for the direct production of pentanoic biofuels starting from neat ethyl levulinate EL), instead of the usually starting molecule LA, using zeolite-supported bifunctional catalysts with confined active site proximity. Compared to the previously reported route based on LA (Route 2 in Scheme 1), the proposed route based on EL (Route 1 in Scheme 1) shows significant advantages: 1) EL can be efficiently produced as the downstream platform molecule via the alcoholysis of lignocellulose materials, wherein humin formation via undesired condensation reactions can be more efficiently suppressed compared to the route based on LA and 2) alleviating the severeness of the reaction medium for catalysts by using a mild ester instead of protic acid as substrate, and thus more feasible for applying higher substrate concentrations or even neat substrate solutions. We present a simple and efficient synthesis method to directly generate highly dispersed ultra-small Ru particles confined in the micropores of zeolite Y. By a combination of state-of-the-art electron microscopy-based techniques and experimental approaches, we found that zeolite-tailored confined proximity between metal and acid sites is pivotal for catalytic performance in the direct HDO of EL into pentanoic biofuels, enabling a remarkable increase in activity and selectivity to pentanoic biofuels. Furthermore, we show that the presence of La in zeolite Y can significantly improve catalyst stability and suppresses zeolite dealumination and desilication during catalysis. Besides, an enhanced understanding of the improved HDO performance of intimacy functional sites behind this reaction, provided by this study, will not only be a step forward in the efficient production of pentanoic biofuels, but it will also aid in understanding similar hydrogenation reactions in tandem catalysis, which may bring a great and multidisciplinary impact in fundamental aspects.

Results and Discussion

For the economical production of pentanoic biofuels (i.e., EP and PA), it is desirable to study the hydrodeoxygenation (HDO) of EL at high substrate concentrations. We have performed the HDO of EL under batch conditions with neat EL as substrate at 220°C and 40 bar H_2. Previous reports have revealed that Ru-based catalyst materials appear as the catalyst of choice for the hydrogenation of LA, owing to the excellent activity and selectivity.[7] A series of state-of-the-art Ru-based catalysts, prepared by a wet impregnation method (see Methods in Supplementary Information and Figure S1), have been rationally screened (Figure 1a). The catalytic screening results demonstrate that controllably depositing Ru nanoclusters inside the 12 MR channels/cages (FAU and BEA) is beneficial for both activity and selectivity. Especially, the level of activity afforded by the Ru/H-Y and Ru/La-Y catalysts has so far
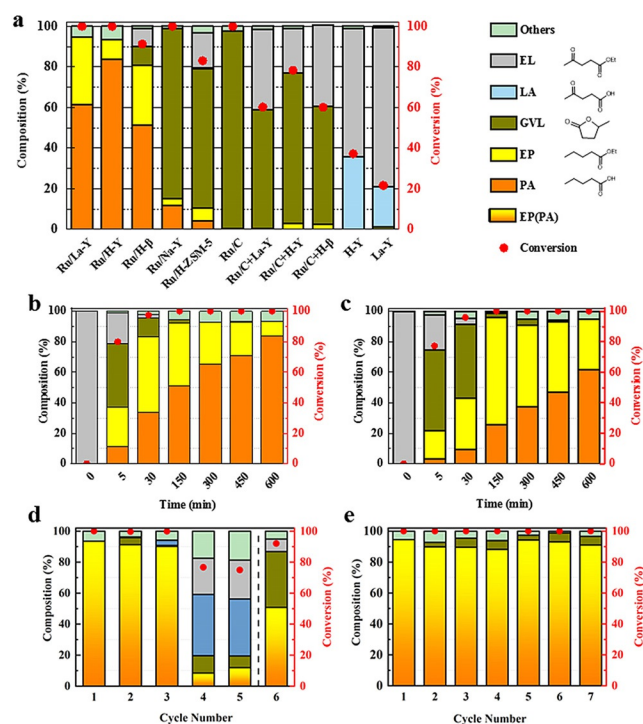
Figure 1. Catalytic performance of the different bifunctional catalysts under study. a) Catalytic hydrodeoxygenation of neat EL over different catalysts after a reaction time of 10 h. b),c) Time profiles of the catalytic hydrodeoxygenation of neat EL over Ru/H-Y and Ru/La-Y, from which the EP/PA productivities of both catalysts were determined at the ca. 100% EL conversion levels at the reaction time of 30 min. d),e) Reusability tests of Ru/H-Y and Ru/La-Y, respectively, the column behind dash line was performed over the regenerated Ru/H-Y catalyst. The sixth run in (d), noted as the column behind dash line was performed over the regenerated Ru/H-Y catalyst. Reaction conditions: 220°C, 40 bar H_2, 1 wt% Ru loading with different supports and a mechanical stirring speed of 1000 rpm. EL: ethyl levulinate; LA: levulinic acid; GVL: γ-valerolactone; EP: ethyl pentanoate; PA: pentanoic acid. The level of activity exhibited by zeolite Y confined Ru nanoparticles has shown to be unique.

23714   www.angewandte.org

© 2021 Wiley-VCH GmbH

*Angew. Chem. Int. Ed.* **2021**, *60*, 23713 – 23721

proven to be unique for the one-pot conversion of EL into EP/PA, as a quantitative conversion of EL and a combined EP/PA yield of $\geq 94\%$ observed for both catalysts after 10 h. The other Ru-based catalysts, such as Ru nanoclusters inside the 10 MR channels (MFI), Ru nanoclusters with less acid sites (Ru/Na-Y and Ru/C), the intimate mixture of Ru nanoclusters and zeolites (Ru/C combined with different zeolites) or other Ru nanoparticles with inferior activity or negligible selectivity towards EP/PA for the HDO of EL, of the confinement of Ru nanoparticles inside zeolite Y for the promotion of catalysis. Furthermore, EP/PA productivity, expressed as the number of EP/PA molecules produced per gram of metal per time, reflects the turnover rate of deep hydrogenation products. Based on the time profiles (Figure 1 b,c and Figure S2), the EP/PA productivities are determined to be $11.514 \, mol \, g_{Ru}^{-1} h^{-1}$ for the Ru/H-Y and $5.965 \, mol \, g_{Ru}^{-1} h^{h-1}$ for the Ru/La-Y respectively, which are both much higher than the current highest values obtained for the 1 wt% Rh/H-β and 1 wt% Ru/H-β (Table S1), reported by the Shell laboratories for the one-pot HDO of EL to EP/PA at a higher reaction temperature of 250°C and reproduced in this work.[8] Encouraged by the promising screening results, the time-on-line concentration profiles of substrate and products for the Ru/H-Y and Ru/La-Y are further performed and shown in Figure 1 b,c. For both catalysts, GVL, PA and EP are detected as the major products, with no pentanediol and methyl-tetrahydrofuran observed. Notably, both the Ru/H-Y and Ru/La-Y can afford a combined EP/PA yield of 37% and 22% even at 5 min under reaction conditions, which is significantly higher than those for previous reported catalysts (EP/PA yield < 1%).[5,7c] Trace amount of 4-hydroxypentanoic acid ester (4-HPE) is also detected at low EL conversion level by GC-MS (Figure S3). The significant enhancement in EP/PA yields at initial stage might indicate an alternative reaction pathway to EP via an intermediate of 4-HPE. At 150 min, both catalysts show a full conversion of EL, with EP and PA as the major products. The Ru/H-Y shows a combined EP/PA yield of 92% and minor amounts of GVL (3%), whereas the Ru/La-Y affords a maximum EP/PA yield of 96% and 3% GVL. After 150 min, a progressive increase in the selectivity towards PA is observed for both catalysts over time, as a result of the consecutive hydrolysis of EP to PA by acid catalysis. Notably, a total EP/PA yield of 94% and 95% could be maintained for the Ru/H-Y and for the Ru/La-Y respectively, even extended to a reaction time of 10 h. Such excellent yields of EP/PA ($\geq 94\%$) and high EP productivities, to the best of our knowledge, are first reported for the direct HDO of neat EL under relatively mild conditions (220°C and 40 bar H_2, under which (Table S1) GVL was normally observed as the dominant product for the bifunctional catalysts in the HDO of EL).

The stability of both Ru/H-Y and Ru/La-Y is examined by performing consecutive runs in the direct HDO of EL into EP/PA (Figure 1 d and e). For the Ru/H-Y, the high EP/PA selectivity and yield are only sustained upon three consecutive 10 h runs. A clear deactivation was observed in the fourth run, with a decrease in the EL conversion from an initial 100% to 77%, and a concomitant drop in EP/PA yields from initial 91% to 9%. Even after a regeneration step

involving coke burning-off at 450°C under a dilute hydrogen flow,[7c] the catalytic performance of Ru/H-Y could only get partially recovered in the sixth run, with the EL conversion of 92% and the EP/PA yield of only 50%, indicating irreversible deactivation of the Ru/H-Y during reactions. Similar deactivation of the 1 wt% Ru/H-ZSM-5 during recycling of LA hydrogenation was also reported, primarily caused by the dealumination of the zeolite support.[9] For the Ru/La-Y, marginal drop in activity and selectivity were observed even upon seven consecutive runs. A full EL conversion and an EP/PA yield of > 90% could be still sustained even in the seventh run, indicating an excellent stability of the Ru/La-Y. The stability tests of both catalysts were also performed at the sub-complete conversion levels (Figure S4). Again, the Ru/H-Y showed an obvious, continuous deactivation, while the Ru/La-Y showed no apparent decrease in both EL conversion and EP/PA yield during reusability tests. The results verify the superior stability of the Ru/La-Y in the HDO of EL.

The composition and nanostructure of both Ru/H-Y and Ru/La-Y, were first characterized by inductively coupled plasma optical emission spectrometer (ICP-OES) and aberration-corrected scanning transmission electron microscopy (AC-STEM). The Ru content was determined to be 1 wt% for both catalysts (Table S2). The high-angle annular dark-field (HAADF) images of the Ru/H-Y and Ru/La-Y samples reveal a high dispersion of ultra-small Ru nanoparticles (around 1.5 nm) located within the zeolite crystals (Figure 2 a–d), although they slightly exceed the size of micropores (roughly 1 nm), as reported previously.[10] H_2 chemisorption results of both Ru/H-Y and Ru/La-Y further corroborate the high dispersion of Ru particles ($D \geq 72\%$), with an average Ru particle size of about 1.5 nm for both samples (Table S3). Additionally, close inspection of X-ray diffraction (XRD) patterns of both Ru-containing zeolites (Figure S5) shows a shift of peaks to a lower 2θ angle after the deposition of Ru, indicating a slight lattice expansion by doping Ru particles inside the cavities of the zeolite. This is also in good accordance with the observed decrease in micropores volume of the zeolite supports after Ru deposition (Table S2). To further discriminate the La and Ru species in the HAADF images, Energy dispersive X-ray spectroscopy (EDX) has been applied for the Ru/La-Y, which confirms an atomic dispersion of La species and highly dispersed Ru clusters in the zeolite Y (Figure 2 e–g and Figure S6g,h).

Complementing the direct and local AC-HAADF-STEM observation, the chemical states and local coordination environment of the zeolite Y supported bifunctional catalysts were characterized by X-ray absorption spectroscopy (XAS). XAS of Ru/H-Y and Ru/La-Y were measured after in situ reduction under H_2. The X-ray absorption near-edge structure (XANES) and extended X-ray absorption fine structure (EXAFS) results are shown in Figure 3 a,b, with the fitting results of EXAFS in Figure S7 and Table S4. Both Ru/H-Y and Ru/La-Y share a comparable chemical valence and coordination of Ru. A slightly higher valence state of Ru species is shown in the Ru/H-Y (Ru^{n+}) than that ($Ru^{\delta+}$) in the Ru/La-Y ($n > \delta \approx 0$), between Ru^0 and Ru^{4+} (Figure 3 a). This is consistent with the X-ray photoelectron spectroscopy results (Figure S8) that a higher binding energy at 281.0 eV,
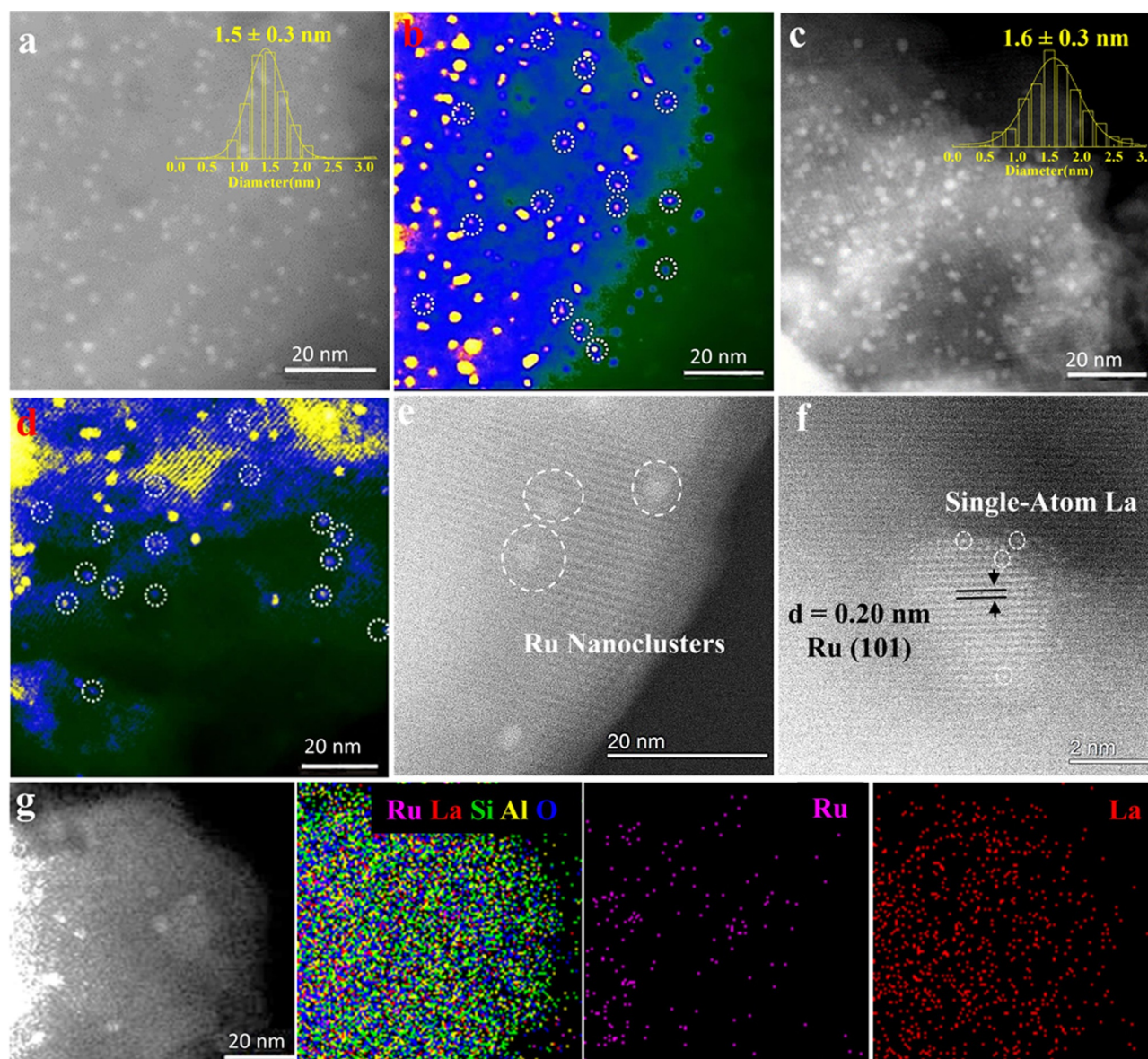
Figure 2. Structural characterization of the bifunctional catalyst materials under study. Representative aberration-corrected high-angle annular dark-field scanning transmission electron microscopy (AC-HAADF-STEM) images of a),b) the Ru/H-Y and c),d) the Ru/La-Y showing the existence of Ru nanoparticles confined in zeolite Y, corresponding particle size distribution derived from measurements of over 200 particles. e),f) Atomic resolution of AC-HAADF-STEM images of the Ru/La-Y and g) EDX spectral imaging of the Ru/La-Y and corresponding elemental maps: Ru pink, La red, Si green, Al yellow, and O blue, showing that Ru and La species are indeed highly dispersed in zeolite Y.

compared to the binding energy of metallic Ru^0 at about 280.6 eV,[11] was shown for the Ru/H-Y, than that at 280.6 eV for the Ru/La-Y. A larger number of Ru-O and a much lower Ru-Ru coordination numbers (CN) with both Ru/H-Y ($CN_{Ru-O} = 3.7 \pm 0.4$, $CN_{Ru-Ru} = 6.0 \pm 0.6$) and Ru/La-Y ($CN_{Ru-O} = 2.8 \pm 0.3$, $CN_{Ru-Ru} = 7.3 \pm 0.6$) samples, as compared to the standard Ru metal foil ($CN_{Ru-O} = 0$, $CN_{Ru-Ru} = 12$), reveal the formation of ultrasmall Ru nanoparticles for both catalysts. Similar values of CN_{Ru-O} and CN_{Ru-Ru} have been reported for the Ru/TiO_2 and $Ru-Pd/TiO_2$, attributed to the formation of a significant fraction of Ru sub-nanometric clusters.[12] Therefore, the XAS results confirm the representative structure of a substantial fraction of Ru ultrasmall nanoparticles or even

clusters in the zeolite Y for the entirety of the both bifunctional catalysts.

The Fourier transform-infrared (FTIR) spectra after CO adsorption for Ru/H-Y and Ru/La-Y catalysts were conducted at −189 °C upon a stepwise increase of CO pressure from sub-mbar to 1 mbar, as shown in Figure 3c and d. For the Ru/H-Y, a feature initially at 2178 cm^{-1} and a red-shift of 10 cm^{-1} are visualized as a function of CO pressure in the sub-mbar range, attributed to CO adsorbed on the protons of H-Y.[13] Notably, a feature at 2128 cm^{-1} develops at a CO partial pressure of above 0.8 mbar, assigned to the multi-coordinated Ru^{n+}-CO according to previous reports.[12] A weak adsorption of Ru^{n+}-CO was indicated in the desorption profile (Figure S9). Interestingly, no observed Ru^0-CO signal suggests

23716 www.angewandte.org

© 2021 Wiley-VCH GmbH

Angew. Chem. Int. Ed. **2021**, 60, 23713 – 23721
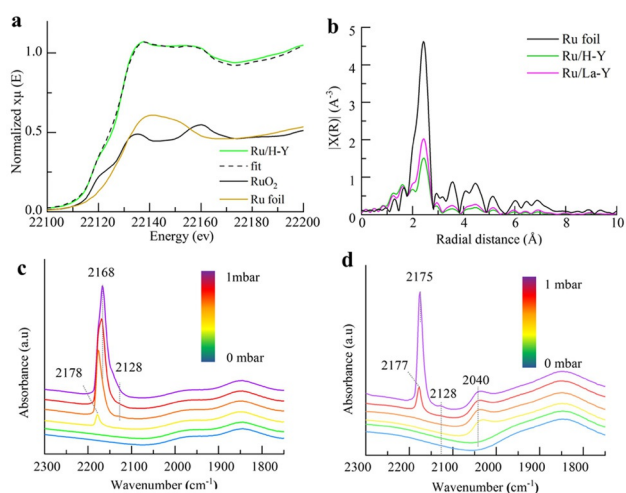
Figure 3. Local environment and electronic feature of Ru nanoparticles. a) Normalized X-ray absorption near edge structure (XANES) of Ru k-edge for Ru foil, RuO_2, Ru/H-Y and Ru/La-Y; b) Fourier transforms of the k^2-weighted extended X-ray absorption fine structure (EXAFS) of Ru K-edge for the Ru foil, Ru/H-Y and Ru/La-Y; c),d) Low-temperature FTIR spectra after CO adsorption on the Ru/H-Y and Ru/La-Y at −189 °C, respectively.

that the Ru particles mainly exhibit a positive charge of Ru^{n+} in the Ru/H-Y. The modulation of the electronic structure of the small Ru nanoparticles confined inside the zeolite is induced by the interaction between the metal species and the zeolite framework. For the Ru/La-Y, a feature initially at 2177 cm^{-1} and a red-shift of 2 cm^{-1} are observed as the adsorbate surface coverage increased, attributed to CO adsorbed on the cations in La-Y.[14] Notably, a feature at 2040 cm^{-1} develops at a relatively low CO pressure of 0.2 mbar, attributed to the linear $Ru^{\delta+}$-CO species.[15] Upon applying high vacuum and heating, the $Ru^{\delta+}$-CO remains up to 100 °C, indicating metallic feature of $Ru^{\delta+}$ with a strong CO adsorption (Figure S9). A weak feature at 2128 cm^{-1} assigned to the multi-coordinated Ru^{n+}-CO is also shown at P_{CO} ≈ 1 mbar. The La modification enriches the Ru nanoparticles in electrons and reduces its effective charge, as also confirmed by XPS and XANES results. This corroborates a degenerated interaction between metal and the zeolite framework after the addition of La cations in zeolite Y, probably caused by the strong electronic interaction between Ru nanoparticles and La species, which is also supported by H_2-TPR (Figure S10). Similar increase in electron charge on Pt clusters via the addition of metal cations has been noted by Visser et al. for their Pt/Y catalyst system.[16]

To clarify the spatial distribution of Ru nanoparticles in FAU zeolites, precision ion polishing system (PIPS) was applied for the preparation of cross-sectional TEM samples. Milling the resin-embedded catalysts with an ion beam produces thin slices exposing the inner parts of catalyst granules, and thus provides information of spatial arrangements of metal particles inside the shaped catalyst bodies (Figure 4a). Figure 4b,c show the inside section of Ru/H-Y and Ru/La-Y. Those sections of both samples clearly show a significant fraction of Ru nanoparticles located inside the zeolite crystals, with an average particle size of around 1.5 nm
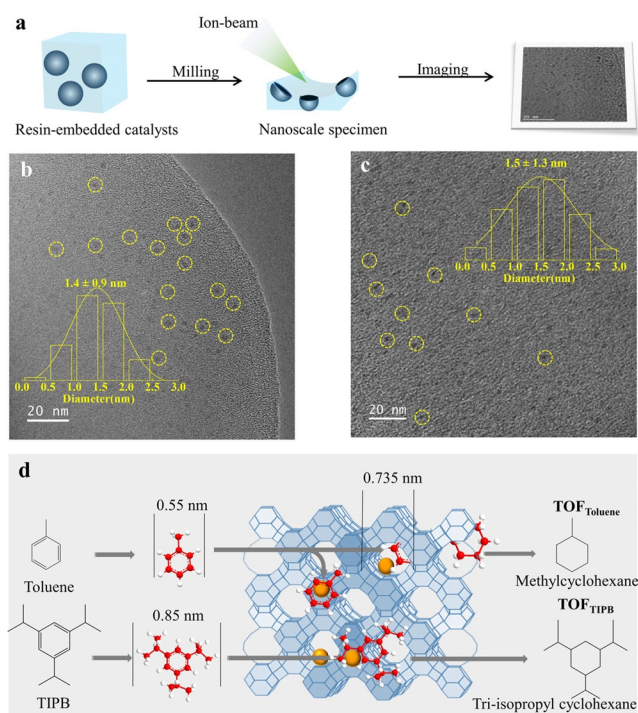
Figure 4. Validation of zeolite-tailored proximity between metal sites and acid sites. a) Diagram of the milling process of resin-embedded catalyst particles with a precision ion polishing system. b),c) TEM images of cross sections of Ru/H-Y and Ru/La-Y respectively. d) Diagram of hydrogenation tests with two probing molecules with different size: toluene (kinetic diameter: 0.55 nm) and 1,3,5-triisopropylbenzene (TIPB, kinetic diameter: 0.85 nm). This reaction process is used to quantify the fraction of Ru nanoclusters constraint inside the zeolite cavities.

for both samples. This is in an excellent agreement with the AC-HAADF-STEM and H_2 chemisorption results. Those indicate that substantial Ru nanoparticles are present inside the cavities of zeolite Y. The sizes of Ru nanoparticles inside the zeolite being slightly larger than the micropores cavities, could be ascribed to the collapse of neighboring cavities during the growth of Ru particles, in a good accordance with previous observation.[10a] XRD results further confirm such changes in the local cavities, as evidenced by the expanding of the zeolite unit cell and a decrease in zeolite crystallinity after metal deposition (Figure S5), probably indicating growth of the Ru particles in a cavity-passing mode.[17]

To further quantify the fraction of such Ru nanoclusters constraint inside the zeolite cavities, we further apply hydrogenation tests with two probing molecules with different size: toluene (kinetic diameter: 0.55 nm, accessible into the cavities of FAU) and 1,3,5-triisopropylbenzene (TIPB, kinetic diameter: 0.85 nm, inaccessible into the cavities of FAU) (Figure 4d and Table S3). The portion of Ru nanoclusters inside the cavities of the zeolite is thus determined to be 78% for the Ru/H-Y and 85% for the Ru/La-Y separately, confirming the validation of most Ru nanoclusters (ca. 1 nm) confined in the micropores of zeolite Y. Consequently, such a significant fraction of Ru nanoclusters encapsulated inside the zeolite cavity provides a sub-nanometric proximity between Ru

particles and acid sites within the confined space provided by the FAU zeolite, which is essential to offer additional benefits in activity for the direct conversion of EL to pentanoic biofuels. Although "the-closer-the-better" with respect to the location of the acid and metal sites, generally recognized for improving activity of the bifunctional catalyst in gas-phase reactions, is challenged for the industrially highly important hydrocracking reaction,[10b] this notion is still advocated for tandem catalysis in the liquid-phase biomass conversion process, as studied in this work.

Our experimental results of the HDO of EL demonstrated that the confined proximity in the zeolite Y supported bifunctional catalysts (Ru/H-Y and Ru/La-Y) has significantly promoted the catalytic activity and selectivity (Figure 1 a). Specifically, when Ru is located inside the FAU zeolite, EL can be quickly hydrogenated to 4-HPE, as evidenced by a significant yield of EP even at an early stage of reaction time (5 min in Figure 1 b, c). Notably, EP/PA are also observed as the dominant products with the Ru/La-Y at a low EL conversion level (with a less amount of catalyst after 30 min in Figure S11). Additionally, 4-HPE, has been detected in GC-MS (Figure S3). Those all point to the occurrence of an alternative pathway of EL-4-HPE-EP. Similar reactive analogue of 4-hydroxypentanoic acid (4-HPA) has been proposed for both thermostatically and electrochemically hydrogenation of LA to PA.[7c, 18] The 4-HPE intermediate might be stabilized by an acid site in zeolite cavities via the confinement and nest effects,[19] and subsequently directly hydrogenated to PE by the adjacent metal site within sub-nanoscale proximity, rather than it being self-ring-closed to GVL on the same acid site. Thus, the rate determining step of GVL ring-opening can be efficiently suppressed. Even with the formation of GVL, GVL ring-opening step can be still facilitated when the metal and acid sites are in a close proximity. Therefore, EP/PA can be produced fast and efficiently even at an early stage of the reaction (Figure 5 a), as consistent with the observed significant EP/PA yields at the initial stage over the zeolite Y supported Ru particles with confined proximity. In the case of the Ru-based bifunctional catalysts with non-confined proximity (Figure 5 b and Figure S11), the yields of EP/PA are generally much lower than that for bifunctional catalysts with confined proximity. The reactive 4-HPE intermediate either cannot be stabilized on the external surface of the zeolite owing to the lack of confinement environment, or quickly hydrolyzed to LA inside the cavity of zeolites and subsequently hydrogenated to GVL when diffusing to the metal sites located on the external surface. Such structure normally results in similarity in product selectivity, with GVL as the dominate product. Accordingly, the FAU zeolite-tailored confined proximity shows an enhanced selectivity towards the production of EP/PA compared to that of the Ru nanoparticles combined with open structure zeolites (Ru/C, Ru/SiO$_2$ or Ru/Al$_2$O$_3$ mixed with H-Y or La-Y in Figure S11 and Table S1), indicating that the confined intimacy sites are the required essential sites for the efficient production of EP/PA in the HDO of EL.

The solid-state ^{1}H MAS NMR spectra of the H-Y, La-Y, Ru/H-Y and Ru/La-Y materials after dehydration are depicted in Figure 6 a. Different zeolitic hydroxyl species can be
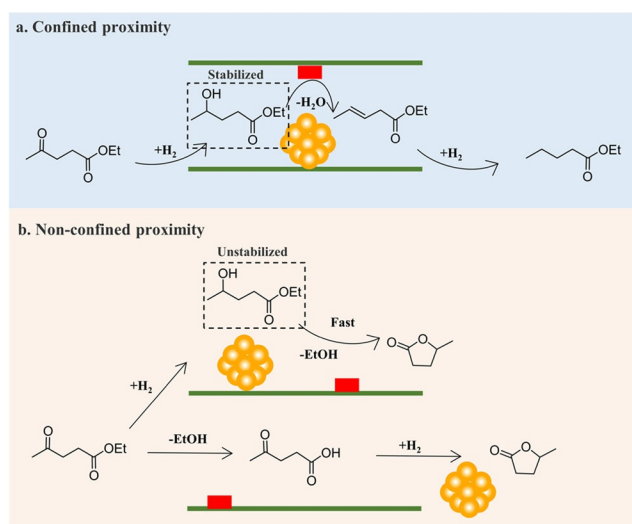
Figure 5. Insight into the proximity effect of the bifunctional catalysts for the hydrodeoxygenation (HDO) of ethyl levulinate (EL). Reaction pathway of selective conversion of EL over bifunctional catalysts a) with confined proximity. b) with non-confined proximity.

discriminated and quantitatively established for all the samples. Four major signals can be discriminated and quantified, assigned to the hydroxyl groups located in the FAU sodalite cages (5.0 ppm) and supercages (3.9 ppm), extra-framework aluminol (2.5 ppm) and non-acidic silanol groups (1.9 ppm) respectively, with two additional minor signals attributed to NH_4^+ species (7.0 ppm) and hydroxyl groups of metal cation (1 ppm that is, Na^+ or Ru).[20] By comparing the La-Y to the H-Y, we find a clear difference in ^{1}H MAS NMR signal patterns. The addition of La into zeolite Y, mainly results in an increase of hydroxyl species in sodalite cages, together with a decrease of the extra-framework Al-OH species. Combining with the atomically dispersed La species in the La-Y determined by AC-HAADF-STEM (Figure 2 f,g and Figure S6g,h), the increase of hydroxyl species in sodalite cages can be attributed to a significant amount of hydroxyl species as charge compensators of La cations, located inside the sodalite cages of the zeolite Y. This is in line with the nature and location of the La species in FAU-type zeolites, as La hydroxylated species majorly in the cavities of FAU topology.[21] After Ru deposition, a decrease of the hydroxyl species in both supercages and sodalite cages was observed for both Ru/H-Y and Ru/La-Y, compared to the parent H-Y and La-Y. This further validates the formation of sub-nanoscale intimacy confined in the cavities of zeolite Y. Notably, the AC-HAADF-STEM of the Ru/La-Y shows that highly dispersed La species closely surrounds the Ru nanoparticles, indicating that La hydroxylated species might provide coordinative sites for Ru species. Combined with the strong interaction between Ru and La species indicated by H$_2$-TPR (Figure S10), the obtained results of probing tests and H$_2$ chemisorption (Table S3) consistently show the La modification further improves the dispersion of Ru species into the cavities of the zeolite Y. It is acknowledged that the rare earth metal modification can be an efficient approach for improving the zeolite stability for gas-phase reactions.[22]
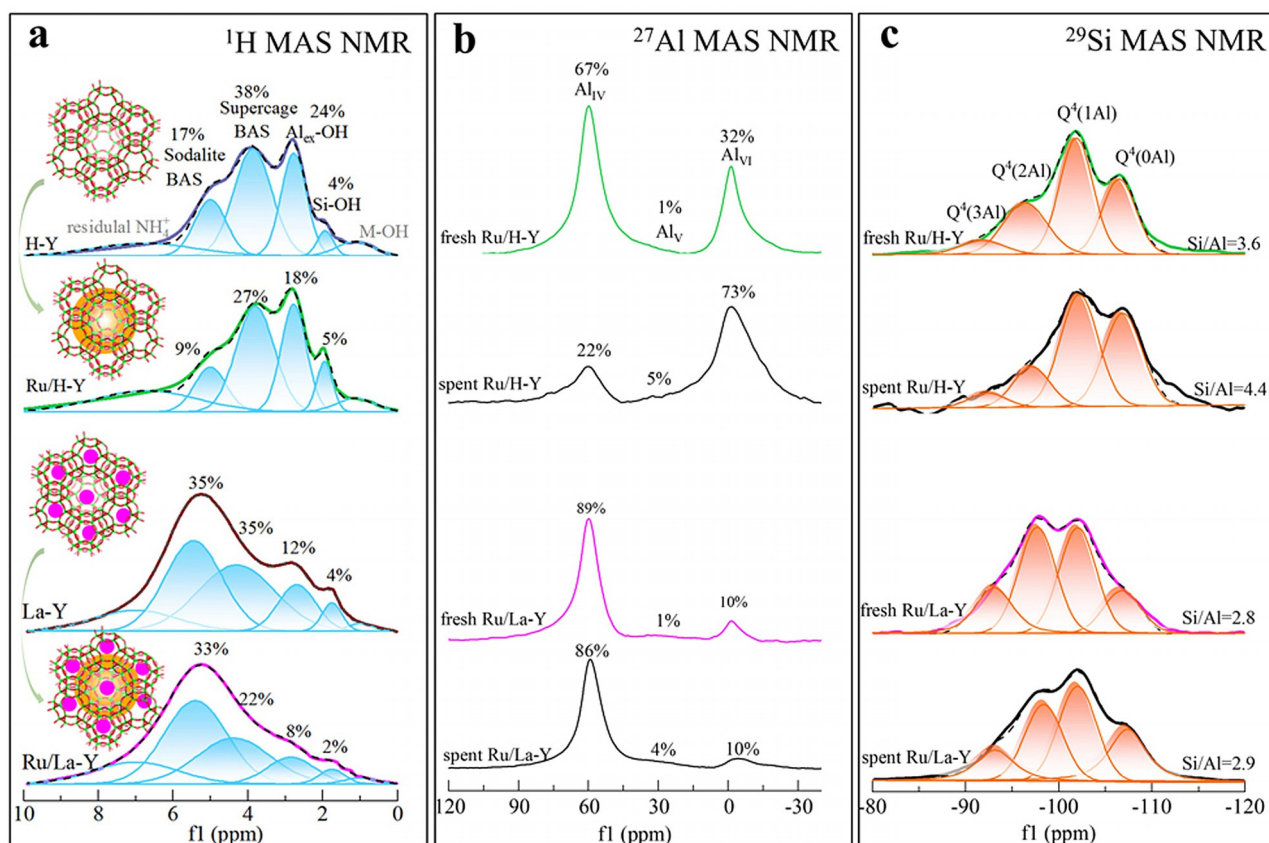
Figure 6. The role of La species on Ru dispersion and catalyst stability. a) ^{1}H MAS NMR spectra of H-Y, Ru/H-Y, La-Y and Ru/La-Y. Relative amounts of each hydroxyl species normalized to the hydroxyl content in the parent zeolite sample; b),c) ^{27}Al and ^{29}Si MAS NMR spectra of fresh and spent Ru/H-Y and Ru/La-Y catalysts (after five consecutive runs), respectively; The solid and dash lines in the NMR spectra represent the measured signals and cumulative peak fitting curve, respectively.

Recently, especially for biomass related liquid phase reactions, dealumination of zeolite materials in liquid phase has been recognized as a major issue for catalyst deactivation. To confirm the validity of a stabilizing effect of La species on EL hydrodeoxygenation, ^{27}Al and ^{29}Si MAS NMR were performed for the fresh and spent Ru/H-Y and Ru/La-Y catalysts. The ^{27}Al MAS NMR spectra (Figure 6b) of all the catalysts show three resonances in the four-coordinated (Al_{IV}), five-coordinated (Al_V) and six-coordinated (Al_{VI}) aluminum region. The Al_{IV} signal at ca. 57 ppm and the Al_{VI} signal at ca. 0 ppm represents tetrahedral framework (FAL) and octahedral extra-framework aluminum (EFAL) species, respectively.[23] Trace amount of the Al_V signal with a broad resonance at around 30 ppm, assigned to EFAL,[24] is also detected for all the catalysts. For the fresh catalysts, the Ru/H-Y shows a FAL of 67% and an EFAL of 32%, while the Ru/La-Y depicts a FAL of 89% and an EFAL of 10%. The more prevalence of tetrahedral FAL in the Ru/La-Y, in line with the dominant Brønsted acid sites (BAS) probed by NH$_3$-TPD and FTIR spectroscopy of adsorbed pyridine results (Table S5 and Figure S12,13), indicates that La modification can efficiently suppress the generation of EFAL species during the preparation processes (i.e. calcination and reduction), which is in a good agreement with ^{1}H MAS NMR. After five consecutive runs, the spent Ru/H-Y clearly shows a significant decrease in

FAL (Al_{IV}) and a simultaneous increase in EFAL (both Al_V and Al_{VI}). The severe dealumination of FAL observed for the spent Ru/H-Y, indicates a severe loss of BAS by 45%, pointing to a severe dealumination of H-Y during the multiple reuse tests, as also evidenced Al leaching by ICP analysis (Table S6). The ^{29}Si MAS NMR results confirm the validation of a severe dealumination occurred for the Ru/H-Y, with an increase of Si/Al ratio from 3.6 to 4.4 during the multiple reuses. Support dealumination accounted for the catalyst deactivation was also reported for the Ru/H-beta and Ru/H-ZSM-5 for the HDO of LA upon multiple reuse under such liquid phase conditions.[7c, 25] Additionally, support desilication has also occurred for the Ru/H-Y during multiple reuses, whilst no Si leaching observed for the Ru/La-Y, as evidenced by ICP analysis (Table S6). Notably, La cations indeed stabilize the FAU zeolite structure and efficiently suppress the deconstruction of FAU zeolites during catalyst preparation and catalysis.[26] Compared to the fresh Ru/La-Y, the spent Ru/La-Y after five consecutive runs, shows only trace amount (3%) of transformation of FAL (Al_{IV}) to EFAL (Al_V), indicating no apparent dealumination of the La-Y. This is also supported by the limit change of Si/Al ratio from 2.8 to 2.9 even after five consecutive runs, shown by ^{29}Si MAS NMR (Figure 6c). The presence of La cations in zeolite Y indeed efficiently prevents the dealumination in the liquid phase

under reaction conditions, which correlates well with no apparent drop in catalyst reactivity even after consecutive runs. Recently, Louwen et al. reported that the presence of La species in the zeolite Y indeed resulted in a higher energy barrier of dealumination, supporting a stabilizing effect of La species on zeolite structure.[27] Furthermore, no apparent leaching of Al and Si species detected by ICP corroborates the stabilizing effect of La species (Table S6). Additionally, the presence of La cations in the Ru/La-Y, significantly alleviates the coke formation during catalysis, as evidenced in thermal gravimetric analysis (Figure S14). Therefore, the excellent stability of the Ru/La-Y for the direct, one-pot conversion of EL to EP/PA can be primarily attributed to the retained structure of the confined proximity by prevention of deconstruction of the zeolite Y during catalysis, implemented by the stabilizing effect of La species in the zeolite.

Conclusion

This work demonstrated the direct hydrodeoxygenation (HDO) of ethyl levulinate (EL) into pentanoic biofuels, catalyzed by zeolite-tailored bifunctional catalyst materials with confined proximity. The Ru-loaded zeolite Y catalysts provide a sub-nanometric proximity between metal and acid sites, located and validated by a combined characterization of advanced electron microscopy, including AC-HAADF-STEM and cross-sectional-TEM, as well as probing tests. The catalysis results show that such confined proximity significantly promotes the catalytic activity and selectivity to the production of pentanoic biofuels in the direct HDO of neat EL. Maintaining such confined proximity is crucial for catalyst stability. La modification is an efficient approach to retain the catalyst performance, owing to stabilizing the zeolite framework against deconstruction during thermocatalysis in the liquid phase. Our findings also extend the notion of "the closer, the better" into biomass catalysis, and such confined proximity in the zeolite cavities enables efficiently coupling of catalytic reactions in a direct, one-pot process, which creates opportunities for the practical production of pentanoic biofuels.

Acknowledgements

Conflict of Interest

The authors declare no conflict of interest.

[1] a) M. Poliakoff, P. Licence, *Nature* **2007**, *450*, 810–812; b) P. E. Brockway, A. Owen, L. I. Brand-Correa, L. Hardt, *Nat. Energy* **2019**, *4*, 612–621; c) A. Corma, S. Iborra, A. Velty, *Chem. Rev.* **2007**, *107*, 2411–2502.

[2] a) C. O. Tuck, E. Pérez, I. T. Horváth, R. A. Sheldon, M. Poliakoff, *Science* **2012**, *337*, 695–699; b) G. W. Huber, S. Iborra, A. Corma, *Chem. Rev.* **2006**, *106*, 4044–4098.

[3] a) D. M. Alonso, S. H. Hakim, S. Zhou, W. Won, O. Hosseinaei, J. Tao, V. Garcia-Negron, A. H. Motagamwala, M. A. Mellmer, K. Huang, C. J. Houtman, N. Labbé, D. P. Harper, C. T. Maravelias, T. Runge, J. A. Dumesic, *Sci. Adv.* **2017**, *3*, e1603301; b) D. Shindell, C. Smith, *Nature* **2019**, *573*, 408–411.

[4] K. Barta, *Nat. Energy* **2018**, *3*, 917–918.

[5] J.-P. Lange, R. Price, P. M. Ayoub, J. Louis, L. Petrus, L. Clarke, H. Gosselink, *Angew. Chem. Int. Ed.* **2010**, *49*, 4479–4483; *Angew. Chem.* **2010**, *122*, 4581–4585.

[6] a) W. Luo, W. Cao, P. C. A. Bruijnincx, L. Lin, A. Wang, T. Zhang, *Green Chem.* **2019**, *21*, 3744–3768; b) Z. Yu, X. Lu, J. Xiong, N. Ji, *ChemSusChem* **2019**, *12*, 3915–3930.

[7] a) W. R. H. Wright, R. Palkovits, *ChemSusChem* **2012**, *5*, 1657–1667; b) L. E. Manzer, *Appl. Catal. A* **2004**, *272*, 249–256; c) W. Luo, P. C. A. Bruijnincx, B. M. Weckhuysen, *J. Catal.* **2014**, *320*, 33–41; d) J. Ftouni, A. Muñoz-Murillo, A. Goryachev, J. P. Hofmann, E. J. M. Hensen, L. Lu, C. J. Kiely, P. C. A. Bruijnincx, B. M. Weckhuysen, *ACS Catal.* **2016**, *6*, 5462–5472; e) T. Pan, J. Deng, Q. Xu, Y. Xu, Q.-X. Guo, Y. Fu, *Green Chem.* **2013**, *15*, 2967–2974.

[8] P. John, V. D. Brink, K. L. V. Hebel, J.-P. Lange, L. Petrus, U.S. Patent 8,003,818; B2, **2011**.

[9] W. Luo, E. R. H. van Eck, P. C. A. Bruijnincx, B. M. Weckhuysen, *ChemPhysChem* **2018**, *19*, 379–385.

[10] a) J. Zečević, A. M. J. van der Eerden, H. Friedrich, P. E. de Jongh, K. P. de Jong, *ACS Nano* **2013**, *7*, 3698–3705; b) J. Zecevic, G. Vanbutsele, K. P. de Jong, J. A. Martens, *Nature* **2015**, *528*, 245–248.

[11] a) C. Elmasides, D. I. Kondarides, W. Grünert, X. E. Verykios, *J. Phys. Chem. B* **1999**, *103*, 5227–5239; b) J. Sun, X. Li, A. Taguchi, T. Abe, W. Niu, P. Lu, Y. Yoneyama, N. Tsubaki, *ACS Catal.* **2014**, *4*, 1–8.

[12] W. Luo, M. Sankar, A. M. Beale, Q. He, C. J. Kiely, P. C. A. Bruijnincx, B. M. Weckhuysen, *Nat. Commun.* **2015**, *6*, 6540.

[13] O. Cairon, T. Chevreau, J. C. Lavalley, *J. Chem. Soc.* **1998**, *94*, 3039–3047.

[14] J. G. Goodwin, C. Naccache, *J. Catal.* **1980**, *64*, 482–486.

[15] Y. Zhang, X. Yang, X. Yang, H. Duan, H. Qi, Y. Su, B. Liang, H. Tao, B. Liu, D. Chen, X. Su, Y. Huang, T. Zhang, *Nat. Commun.* **2020**, *11*, 3185.

[16] T. Visser, T. A. Nijhuis, A. M. J. van der Eerden, K. Jenken, Y. Ji, W. Bras, S. Nikitenko, Y. Ikeda, M. Lepage, B. M. Weckhuysen, *J. Phys. Chem. B* **2005**, *109*, 3822–3831.

[17] K. Cheng, L. I. van der Wal, H. Yoshida, J. Oenema, J. Harmel, Z. Zhang, G. Sunley, J. Zečević, K. P. de Jong, *Angew. Chem. Int. Ed.* **2020**, *59*, 3592–3600; *Angew. Chem.* **2020**, *132*, 3620–3628.

[18] a) J. C. Serrano-Ruiz, R. M. West, J. A. Dumesic, *Annu. Rev. Chem. Biomol.* **2010**, *1*, 79–100; b) L. Xin, Z. Zhang, J. Qi, D. J. Chadderdon, W. Li, *ChemSusChem* **2013**, *6*, 674–686.

[19] L. Liu, A. Corma, *Nat. Rev. Chem.* **2021**, *5*, 256—276.

[20] a) J. Klinowski, *Chem. Rev.* **1991**, *91*, 1459–1479; b) G. Paul, C. Bisio, I. Braschi, M. Cossi, G. Gatti, E. Gianotti, L. Marchese, *Chem. Soc. Rev.* **2018**, *47*, 5684–5739; c) B. H. Wouters, T. Chen, P. J. Grobet, *J. Phys. Chem. B* **2001**, *105*, 1135–1139; d) B. H. Wouters, T. H. Chen, P. J. Grobet, *J. Am. Chem. Soc.* **1998**, *120*, 11419–11425.

[21] F. Schüßler, E. A. Pidko, R. Kolvenbach, C. Sievers, E. J. M. Hensen, R. A. van Santen, J. A. Lercher, *J. Phys. Chem. C* **2011**, *115*, 21763–21776.

[22] E. T. C. Vogt, B. M. Weckhuysen, *Chem. Soc. Rev.* **2015**, *44*, 7342–7370.

[23] a) J. A. Van Bokhoven, A. L. Roest, D. C. Koningsberger, J. T. Miller, G. H. Nachtegaal, A. P. M. Kentgens, *J. Phys. Chem. B* **2000**, *104*, 6743–6754; b) J. W. Roelofsen, H. Mathies, R. L. de Groot, P. C. M. van Woerkom, H. A. Gaur, *Stud. Surf. Sci. Catal.* **1986**, *28*, 337–344; c) J. Kanellopoulos, A. Unger, W. Schwieger, D. Freude, *J. Catal.* **2006**, *237*, 416–425.

[24] J. Chen, T. Chen, N. Guan, J. Wang, *Catal. Today* **2004**, *93–95*, 627–630.

[25] W. Luo, U. Deka, A. M. Beale, E. R. H. V. Eck, P. C. A. Bruijnincx, B. M. Weckhuysen, *J. Catal.* **2013**, *301*, 175–186.

[26] S. Yu, J. Yan, W. Lin, J. Long, S. Liu, *Catal. Lett.* **2021**, *151*, 698–712.

[27] J. N. Louwen, S. Simko, K. Stanciakova, R. E. Bulo, B. M. Weckhuysen, E. T. C. Vogt, *J. Phys. Chem. C* **2020**, *124*, 4626–4636.